INTERNATIONAL JOURNAL OF STATISTICAL ANALYSIS

ISSN: 2690-2265
ACCEPTED: 25.11.2026
PUBLISHED: 26.11.2026

COMPARATIVE EVALUATION OF IMAGE DENOISING METHODS FOR MEDICAL IMAGE PROCESSING

Ibrokhimbek Yusupov

Mukhriddin Abduganiev

Jakhongirbek Latipov

Tashkent University of Information Technologies named after Muhammad al-Khwarizmi, Uzbekistan

Abstract

This study presents a comparative evaluation of seven classical image denoising algorithms for reducing Rician noise in brain MRI images. Gaussian, Median, Bilateral, Perona–Malik, Total Variation, Wavelet, and Non-Local Means filters were evaluated at five noise levels. Their performance was assessed using Peak Signal-to-Noise Ratio (PSNR), Structural Similarity Index (SSIM), and processing time. The results indicate that Non-Local Means achieves the highest PSNR values, while Total Variation provides strong structural preservation. Gaussian filtering demonstrates the lowest computational cost. These findings highlight the trade-offs between denoising quality, structural preservation, and computational efficiency.

Keywords

medical image processing, noise, Gaussian filter, image denoising, image quality assessment, structural preservation, computational efficiency.

Introduction

The rapid advancement of medical imaging technologies worldwide has significantly increased the potential for early disease detection and improved treatment effectiveness. Imaging systems such as computed tomography (CT), magnetic resonance imaging (MRI), and ultrasound (US) enable the high-resolution visualization of anatomical structures [1,16]. However, the quality of acquired images depends on numerous internal and external factors. Technical parameters of imaging equipment, patient motion, noise, slice thickness, contrast agent distribution, and imaging protocols may all affect the diagnostic value of the resulting images [2,3].

https://creativecommons.org/licenses/by/4.0/

ISSN: 2690-2265
ACCEPTED: 25.11.2026
PUBLISHED: 26.11.2026

In particular, the quality of MRI images is largely determined by the signal-to-noise ratio (SNR). Since MRI image formation involves the acquisition of the magnitude of a complex-valued signal, the resulting noise follows a Rician distribution [4]. This phenomenon introduces a positive bias in low-signal regions, making it difficult to identify fine anatomical structures and potentially degrading the performance of subsequent automated image analysis procedures [5]. When working with low-resolution images, it is also necessary to exploit the available information to reconstruct higher-quality images through digital image processing techniques [6,7]. Therefore, image preprocessing and noise reduction constitute essential steps before subsequent analysis.

Numerous scientific studies have investigated methods for removing noise from medical images. Various filtering and digital image processing techniques have been developed for this purpose. These include spatial linear and nonlinear filters, such as Gaussian and median filters; edge-preserving adaptive filters, including bilateral filtering and Perona–Malik anisotropic diffusion; variational models, particularly Total Variation (TV); and patch-based Non-Local Means (NLM) methods. However, a review of the relevant literature indicates that most of these methods have been evaluated under different experimental conditions and using different datasets. Consequently, their comparative performance under identical experimental conditions has not been sufficiently investigated.

The objective of this study is to analyze classical denoising methods under a unified experimental framework, using an identical Rician noise model and standardized parameter settings, and to identify an appropriate balance between image restoration accuracy and computational efficiency.

The experiments were conducted using T1-weighted brain MRI images obtained from the open-access Figshare database. From the dataset comprising 766 high-resolution axial and sagittal images in **.mat* format, 110 images corresponding to 56 patients were randomly selected for experimental evaluation. Of these, 10 images

https://creativecommons.org/licenses/by/4.0/

INTERNATIONAL JOURNAL OF STATISTICAL ANALYSIS
ISSN: 2690-2265
ACCEPTED: 25.11.2026
PUBLISHED: 26.11.2026

were allocated to the parameter optimization subset, while the remaining 100 images were used for the final evaluation and comparison of algorithm performance.

All images were normalized in terms of intensity values and used as reference images.

For each filtering method and each noise level $\boldsymbol{\sigma}$, a parameter grid $\boldsymbol{k}$ was evaluated using the 10 images in the validation subset. The parameter value that maximized the average PSNR was selected (Table 1). The selected parameter values were then applied unchanged to the 100 test images.

Table 1. *Optimal parameter values selected using the validation subset.*

Method	**σ = 1%**	**σ = 3%**	**σ = 5%**	**σ = 7%**	**σ = 9%**
Gaussian (std)	0.5	0.8	0.8	1.0	1.0
Median (window)	3	3	3	3	5
Bilateral (k)	0.5	1	2	2	2
Perona–Malik (k)	1	2	2	2	2
TV (k)	0.5	1	1	1	1
NLM (k)	1	1	1	1	1

All experiments were conducted using the Google Colab cloud-based computational environment running on Linux (kernel version 6.6.159+). The allocated computational resources consisted of a virtual CPU with two logical cores and 12.67 GB of RAM. All experiments were implemented in Python 3.13.18.

The image processing and scientific computing operations were performed using NumPy 2.4.6, SciPy 1.16.3, Scikit-image 0.25.2, and OpenCV 4.14.0. PyTorch version 2.11.0+cpu was also installed in the computational environment.

Since MRI scanners acquire the magnitude of a complex-valued signal, the resulting noise follows a Rician distribution [8]. To simulate realistic clinical imaging conditions, artificial Rician noise was added to the normalized reference images at controlled noise levels. It can be mathematically expressed as follows:

$$z(x,y) = \sqrt{\left(I_{ref}(x,y) + n_1(x,y)\right)^2 + n_2(x,y)^2} \qquad (1)$$

https://creativecommons.org/licenses/by/4.0/

INTERNATIONAL JOURNAL OF STATISTICAL ANALYSIS
ISSN: 2690-2265
ACCEPTED: 25.11.2026
PUBLISHED: 26.11.2026

Here, $n_1, n_2 \sim \mathcal{N}(0, \sigma^2)$ represents mutually independent Gaussian random variables with zero mean and variance σ^2. The noise level was simulated at $\sigma = (1\%, 3\%, 5\%, 7\%, 9\%)$ levels on a normalized scale.

In this study, the performance of seven classical filtering algorithms was investigated by applying them to noisy images under identical experimental conditions.

1. Gaussian Filter

The Gaussian filter is a spatial linear smoothing operator that replaces each pixel with a weighted average of the surrounding pixel values:

$$I_{Gauss}(x,y) = \frac{1}{2\pi\sigma_g^2} \iint I\,(u,v) \exp\left(-\frac{(x-u)^2+(y-v)^2}{2\sigma_g^2}\right) du\, dv \qquad (2)$$

This filtering method effectively smooths image noise. However, it may blur anatomical boundaries and contours, resulting in the loss of fine structural details.

2. Median Filter

The median filter is a nonlinear spatial filtering technique that sorts the pixel values within a selected neighborhood window and replaces the central pixel with the median value:

$$I_{Median}(x,y) = \text{median}\{I(u,v) \mid (u,v) \in W(x,y)\} \qquad (3)$$

The median filter is primarily effective in removing impulse noise. However, it may also eliminate fine structural details of biological tissues.

3. Bilateral Filter

The bilateral filter [9] is a nonlinear edge-preserving filtering technique that simultaneously considers spatial distance and differences in pixel intensity:

$$I_{Bilateral}(x) = \frac{1}{W_p} \sum_{x_i \in \Omega} I\,(x_i) g_s(\|x_i - x\|) g_r(|I(x_i) - I(x)|) \qquad (4)$$

Here g_s — denotes the spatial Gaussian kernel, g_r — represents the range (intensity) Gaussian kernel, and W_p — s the normalization coefficient.

4. Perona–Malik Anisotropic Diffusion

https://creativecommons.org/licenses/by/4.0/

INTERNATIONAL JOURNAL OF STATISTICAL ANALYSIS
ISSN: 2690-2265
ACCEPTED: 25.11.2026
PUBLISHED: 26.11.2026

Perona–Malik anisotropic diffusion is a partial differential equation-based approach [10] that controls the diffusion process according to the local image gradient:

$$\frac{\partial I}{\partial t} = \text{div}(c(\|\nabla I\|)\nabla I) \quad (5)$$

The conduction function $c(k)$ suppresses diffusion in high-gradient regions corresponding to image boundaries:

$$c(\|\nabla I\|) = \exp\left(-\left(\frac{\|\nabla I\|}{\kappa}\right)^2\right) \quad (6)$$

5. Total Variation

The Rudin–Osher–Fatemi (ROF) variational model [11] performs image smoothing by minimizing the total variation of the image:

$$\underset{I}{\text{Min}} \int_\Omega \|\nabla I\| \, dxdy + \lambda \int_\Omega (I - z)^2 \, dxdy \quad (7)$$

This model effectively removes noise in homogeneous regions while preserving image boundaries and sharp structural transitions [7].

6. Bayes Shrink Wavelet Thresholding

This method transforms the image into the wavelet domain and applies adaptive soft thresholding based on Bayesian estimation:

$$T_{Bayes} = \frac{\sigma^2_{noise}}{\sigma_{signal}} \quad (8)$$

The wavelet coefficients in the corresponding subbands are processed using the selected T_{Bayes} threshold, followed by an inverse wavelet transform to reconstruct the denoised image [12].

7. Non-Local Means (NLM)

The Non-Local Means method [13,14] identifies similar pixel patches throughout the image using a global search strategy and calculates a weighted average of their intensity values:

$$I_{NLM}(i) = \sum_{j\in\Omega} w(i,j)I(j), \quad w(i,j) = \frac{1}{Z(i)} \exp\left(-\frac{\|N_i - N_j\|^2_{2,a}}{h^2}\right) \quad (9)$$

https://creativecommons.org/licenses/by/4.0/

INTERNATIONAL JOURNAL OF STATISTICAL ANALYSIS
ISSN: 2690-2265
ACCEPTED: 25.11.2026
PUBLISHED: 26.11.2026

Here N_i and N_j — denote the image patches surrounding pixels i and j , respectively, while h represents the filtering parameter.

The difference between the filtered image $K(x,y)$ and the reference image $I_{ref}(x,y)$ was evaluated within the brain mask Ω using two principal metrics. Peak Signal-to-Noise Ratio (PSNR) was employed to quantify the pixel-wise reconstruction error between the denoised image and the corresponding reference image [15]. It can be calculated using the following expression:

$$\text{MSE} = \frac{1}{|\Omega|}\sum_{(x,y)\in\Omega}\left(I_{ref}(x,y) - K(x,y)\right)^2 \qquad (10)$$

$$\text{PSNR} = 10 \cdot \log_{10}\left(\frac{\text{MAX}_I^2}{\text{MSE}}\right) \qquad (11)$$

here, $MAX_I = 1.0$ represents the maximum possible pixel value of the image.

The Structural Similarity Index Measure (SSIM) was used to evaluate the structural integrity of the reconstructed images. It is calculated according to the following expression:

$$\text{SSIM}(x,y) = \frac{(2\mu_x\mu_y+c_1)(2\sigma_{xy}+c_2)}{(\mu_x^2+\mu_y^2+c_1)(\sigma_x^2+\sigma_y^2+c_2)} \qquad (12)$$

here, μ denotes the mathematical expectation (mean value), σ^2 represents the variance, $\sigma_{I,final}$ denotes the covariance, and, C_1 and C_2 are stabilizing constants.

The experimental results demonstrate that the evaluated filtering methods improved the PSNR and SSIM values relative to the noisy images in most experimental conditions. Table 2 presents the average PSNR values achieved at different noise levels.

Table 2. *Performance of filtering methods at different noise levels in terms of PSNR.*

Method	**σ = 1%**	**σ = 3%**	**σ = 5%**	**σ = 7%**	**σ = 9%**
Noisy (baseline)	40.01 ± 0.02	30.50 ± 0.02	26.09 ± 0.02	23.20 ± 0.02	21.05 ± 0.03
Gaussian	41.98 ± 0.63	35.55 ± 1.02	32.68 ± 0.66	30.32 ± 0.85	28.31 ± 0.79
Median	39.63 ± 1.13	35.06 ± 0.57	31.79 ± 0.41	29.22 ± 0.37	27.74 ± 0.82

https://creativecommons.org/licenses/by/4.0/

INTERNATIONAL JOURNAL OF STATISTICAL ANALYSIS

ISSN: 2690-2265
ACCEPTED: 25.11.2026
PUBLISHED: 26.11.2026

Bilateral	40.07 ± 0.09	31.75 ± 0.30	28.11 ± 0.47	26.08 ± 0.50	24.56 ± 0.54
Perona–Malik	40.53 ± 0.26	33.14 ± 0.56	30.66 ± 0.71	28.96 ± 0.86	27.45 ± 0.93
TV	42.53 ± 0.34	35.69 ± 0.58	32.55 ± 0.62	30.22 ± 0.67	28.22 ± 0.74
Wavelet	41.28 ± 0.22	33.64 ± 0.35	30.39 ± 0.45	28.28 ± 0.53	26.61 ± 0.60
NLM	**42.58 ± 0.49**	**36.26 ± 0.59**	**33.13 ± 0.57**	**30.65 ± 0.63**	**28.52 ± 0.74**

The results presented in Table 2 indicate that the Non-Local Means method achieved the highest PSNR values among the evaluated algorithms across all noise levels. However, an analysis based on the SSIM metric, which evaluates structural similarity, revealed that the Total Variation model demonstrated comparatively better structural preservation, particularly at higher noise levels (Table 3).

Table 3. *Structural similarity (SSIM) values of the resulting images*.

Method	**σ = 1%**	**σ = 3%**	**σ = 5%**	**σ = 7%**	**σ = 9%**
Noisy (baseline)	0.963 ± 0.006	0.778 ± 0.028	0.608 ± 0.038	0.486 ± 0.039	0.398 ± 0.037
Gaussian	0.982 ± 0.002	0.946 ± 0.005	0.887 ± 0.012	0.855 ± 0.013	0.800 ± 0.019
Median	0.981 ± 0.002	0.931 ± 0.006	0.857 ± 0.014	0.777 ± 0.022	0.786 ± 0.015
Bilateral	0.966 ± 0.005	0.842 ± 0.013	0.781 ± 0.011	0.699 ± 0.012	0.627 ± 0.013
Perona–Malik	0.973 ± 0.003	0.929 ± 0.008	0.893 ± 0.011	0.859 ± 0.014	0.826 ± 0.017
TV	0.985 ± 0.001	**0.950 ± 0.005**	**0.911 ± 0.007**	**0.868 ± 0.009**	**0.827 ± 0.012**
Wavelet	0.977 ± 0.003	0.895 ± 0.011	0.826 ± 0.016	0.771 ± 0.018	0.726 ± 0.018
NLM	**0.985 ± 0.002**	0.946 ± 0.006	0.905 ± 0.010	0.862 ± 0.014	0.818 ± 0.017

Furthermore, to assess the computational complexity of the investigated methods, the average processing time required to process a single image was measured in seconds and reported separately in Table 4.

Table 4. *Average processing time required by each filtering method to process a single image*.

https://creativecommons.org/licenses/by/4.0/

INTERNATIONAL JOURNAL OF STATISTICAL ANALYSIS
ISSN: 2690-2265
ACCEPTED: 25.11.2026
PUBLISHED: 26.11.2026

Method	Processing time (s)
Gaussian	0.007 ± 0.001
Wavelet	0.020 ± 0.003
Median	0.052 ± 0.006
TV	0.117 ± 0.044
Perona–Malik	0.293 ± 0.063
NLM	0.551 ± 0.127
Bilateral	0.667 ± 0.196

The experimental findings indicate that the optimal denoising method depends on the primary quality criterion, whether pixel-wise reconstruction accuracy or structural integrity is prioritized. The NLM method demonstrated superior performance in reducing image noise (Figure 1). However, its computational cost was found to be higher than that of the other methods.

Specifically, the average processing time required for a single image was 0.007 seconds for the Gaussian filter, 0.117 seconds for the TV model, and 0.551 seconds for the NLM algorithm. Therefore, the use of Total Variation or conventional Gaussian filtering methods is scientifically justified in resource-constrained environments and real-time systems requiring rapid image analysis.

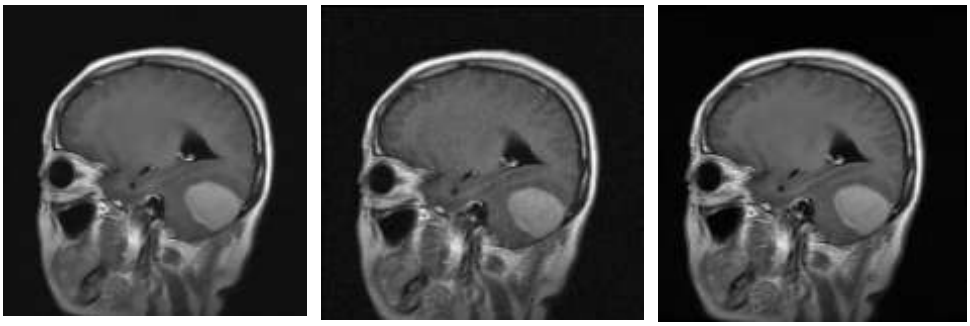

Original reference image | Noisy image | Image processed using the NLM algorithm.

Figure 1. Comparison of the original, noisy, and NLM-denoised images.

This study provides a comprehensive evaluation of seven classical filtering algorithms designed to remove Rician noise from 100 brain MRI images obtained from an open-access dataset under a unified experimental framework.

https://creativecommons.org/licenses/by/4.0/

ISSN: 2690-2265
ACCEPTED: 25.11.2026
PUBLISHED: 26.11.2026

The experimental results and quantitative analyses demonstrate that the selection of an optimal filtering method depends directly on the scientific and practical performance criterion considered. Furthermore, the evaluation of computational complexity and processing speed identified several balanced solutions that may be particularly relevant to real-time diagnostic systems.

The results obtained in this study can serve as a relevant baseline for further investigations. Nevertheless, the study has several methodological limitations. These include the use of clinical MRI images without corresponding noise-free reference images, the optimization of algorithm parameters exclusively based on the PSNR metric, and the absence of a separate clinical evaluation of the effects of the investigated algorithms on subsequent automated segmentation and diagnostic performance.

Based on these limitations, future research will focus on extending the current set of classical filtering methods with modern deep learning architectures and hybrid modeling techniques. Furthermore, practical investigations will be conducted to evaluate the impact of the processed images on the accuracy of automated clinical diagnosis.

Funding

Prepared in relation to the work carried out within the framework of the applied research project at TUIT (Tashkent University of Information Technologies) project № AL-9925025542, titled “Algorithms and Software Suite for Digital Processing of Medical Images and Object Recognition” - covering the period 2026–2028.

References

1. Abduganiev, M., Azimov, R., Muydinov, L. (2023). Digital Processing Algorithms of Biomedical Signals Using Cubic Base Splines. In: Zaynidinov, H., Singh, M., Tiwary, U.S., Singh, D. (eds) Intelligent Human Computer Interaction. IHCI 2022. Lecture Notes in Computer Science, vol 13741. Springer, Cham. https://doi.org/10.1007/978-3-031 27199-1_3

https://creativecommons.org/licenses/by/4.0/

ISSN: 2690-2265
ACCEPTED: 25.11.2026
PUBLISHED: 26.11.2026

2. Zaynidinov, X. N., Baxromov, S. A., & Azimov, B. R. (2019). Biomeditsina signallarini interpolyatsion kubik splayn modellarini qurish. Muhammad al-Xorazmiy avlodlari, 4(10), 14–17.

3. Zaynidinov, H. N., Azimov, B. R., & Abduganiyev, M. M. (2022). Funksiyalarni tiklashda bo‘lak-polinomial usullar tahlili. Academic Research in Educational Sciences, 3(5), 1092–1101. https://doi.org/10.24412/2181-1385-2022-5-1092-1101

4. Zaynidinov, H., Juraev, U., Tishlikov, S., & Modullayev, J. (2024). Application of Daubechies Wavelets in Digital Processing of Biomedical Signals and Images. In Intelligent Human Computer Interaction. Lecture Notes in Computer Science, Vol. 14531, pp. 194–206. Springer. https://doi.org/10.1007/978-3-031-53827-8_19

5. Abduganiev, M. M., Latipov, J. T. (2025, July). Algorithms For Improving The Quality Of Images Using Histogram Method. In International Conference on Global Trends and Innovations in Multidisciplinary Research (Vol. 1, No. 1, pp. 26-33).

6. Hakimjon Z., Bunyod A., Muslim K., Mukhriddin A. (2023). Analysis of accuracy of cubic spline functions using analytic functions. “Innovations in Technology and Science Education”, 2(15), 346-355.

7. Zaynidinov, H. N., Gofurjonov, M. R., Xuramov, L. Y., Pisetskiy, Y. V., & Tojiboev, G. O. (2026). Digital Biomedical Image Processing Using Advanced Digital Hybrid Filters. In Proceedings of International Conference on Computational Intelligence and Information Retrieval, pp. 265–276. Springer.

8. Gudbjartsson, H., & Patz, S. (1995). The Rician distribution of noisy MRI data. Magnetic Resonance in Medicine, 34(6), 910–914. https://doi.org/10.1002/mrm.1910340618

9. Tomasi, C., & Manduchi, R. (1998). Bilateral filtering for gray and color images. In Proceedings of the Sixth IEEE International Conference on Computer Vision (ICCV) (pp. 839–846). https://doi.org/10.1109/ICCV.1998.710815

https://creativecommons.org/licenses/by/4.0/

ISSN: 2690-2265
ACCEPTED: 25.11.2026
PUBLISHED: 26.11.2026

10. Perona, P., & Malik, J. (1990). Scale-space and edge detection using anisotropic diffusion. IEEE Transactions on Pattern Analysis and Machine Intelligence, 12(7), 629–639. https://doi.org/10.1109/34.56205

11. Rudin, L. I., Osher, S., & Fatemi, E. (1992). Nonlinear total variation based noise removal algorithms. Physica D: Nonlinear Phenomena, 60(1–4), 259–268. https://doi.org/10.1016/0167-2789(92)90242-F

12. Chang, S. G., Yu, B., & Vetterli, M. (2000). Adaptive wavelet thresholding for image denoising and compression. IEEE Transactions on Image Processing, 9(9), 1532–1546. https://doi.org/10.1109/83.862633

13. Buades, A., Coll, B., & Morel, J.-M. (2005). A non-local algorithm for image denoising. In Proceedings of the IEEE Computer Society Conference on Computer Vision and Pattern Recognition (CVPR) (Vol. 2, pp. 60–65). https://doi.org/10.1109/CVPR.2005.38

14. Coupé, P., Yger, P., Prima, S., Hellier, P., Kervrann, C., & Barillot, C. (2008). An optimized blockwise nonlocal means denoising filter for 3-D magnetic resonance images. IEEE Transactions on Medical Imaging, 27(4), 425–441. https://doi.org/10.1109/TMI.2007.906087

15. Wang, Z., Bovik, A. C., Sheikh, H. R., & Simoncelli, E. P. (2004). Image quality assessment: From error visibility to structural similarity. IEEE Transactions on Image Processing, 13(4), 600–612. https://doi.org/10.1109/TIP.2003.819861

16. Cheng, J., Huang, W., Cao, S., Yang, R., Yang, W., Yun, Z., Wang, Z., & Feng, Q. (2015). Enhanced performance of brain tumor classification via tumor region augmentation and partition. PLOS ONE, 10(10), e0140381. https://doi.org/10.1371/journal.pone.0140381

17. Rakhimjonovich, A. B., & Mukhriddin, A. A. (2023). DIGITAL PROCESSING OF BIOMEDICAL SIGNALS USING PIECE-POLYNOMIAL METHODS. Central Asian Research Journal for Interdisciplinary Studies (CARJIS), (8 (20)), 510-518..

https://creativecommons.org/licenses/by/4.0/

ISSN: 2690-2265
ACCEPTED: 25.11.2026
PUBLISHED: 26.11.2026

18. Зайнидинов, Х. Н., Азимов, Б. Р., & Абдуғаниев, М. М. Ў. (2022). ФУНКЦИЯЛАРНИ ТИКЛАШДА БЎЛАК-ПОЛИНОМИАЛ УСУЛЛАР ТАХЛИЛИ. Academic research in educational sciences, 3(5), 1092-1101.

19. Azimov, B., Makhmudjanov, S., Badhan, A. K., Abduganiev, M., & Singh, A. (2025, December). Arduino-Controlled Hybrid Optical–RF Sensor Node for Energy-Aware Structural Health Monitoring. In *2025 Optical Communication, Photonics, Telecommunications, and Intelligent Machine Applications (OPTIMA)* (pp. 250-256). IEEE.

20. Abdualimov, F., Abdufattokhov, S., Abduganiev, M., Abdulkhayev, N., Abdullaev, R. Z., Abdumajidovich, Z. A., ... & Eshchanova, N. (2025, December). Abdohwr, Rehaam, 360. In *IEEE Conference ID* (Vol. 67660, pp. 4th-5th).

21. ogli Abduganiev, M. M., & ogli Latipov, J. T. (2025, July). Algorithms For Improving The Quality Of Images Using Histogram Method. In *International Conference on Global Trends and Innovations in Multidisciplinary Research* (Vol. 1, No. 1, pp. 26-33).

22. Azimov, B., Ahmadaliev, B., & Abduganiev, M. (2026, May). Creating a bivariate spline function model and applying it to real data. In *AIP Conference Proceedings* (Vol. 3447, No. 1, p. 020009). AIP Publishing LLC.

23. Abduganiev, M., & Gafurov, S. Application of Two Variable Hermite Splines in Digital Image Processing. *Scientific Collection «InterConf+»*, (34), 308-320.

24. Abdurahmanov, M., Abduganiev, M., Artikova, S., & Nasriddinov, S. Algorithms for Extracting the Image of Stomach Ulcer From the Video Image Recorded by the Endoscope Devices. *Scientific Collection «InterConf»*, (176), 141-145.

https://creativecommons.org/licenses/by/4.0/